


Article

Design of a Dual-Mode Input Structure for K/Ka-Band Gyrotron TWT

Mengshi Ma¹, Qixiang Zhao^{1,*}, Kunshan Mo¹, Shuquan Zheng¹, Lin Peng¹, You Lv¹ and Jinjun Feng² 

¹ School of Information and Communication, Guilin University of Electronic Technology, Guilin 541004, China; m1654259600@163.com (M.M.); mokunshan@126.com (K.M.); sqzheng1120@163.com (S.Z.); penglin@guet.edu.cn (L.P.); lvyoumail@yeah.net (Y.L.)

² National Key Laboratory of Science and Technology on Vacuum Electronics, Beijing Vacuum Electronics Research Institute, Beijing 100015, China; fengjinjun@tsinghua.org.cn

* Correspondence: zxqi@guet.edu.cn; Tel.: +86-13-708-182-612

Abstract: A dual-band gyrotron traveling wave amplifier (Gyro-TWT) can reduce the size, cost, and weight of a transmitter in dual-band radar and communication systems. In this paper, a dual-mode input coupler for K/Ka dual-band gyrotron traveling wave amplifier (Gyro-TWT) is designed. This structure is composed of two different types of input couplers, one is the coaxial input coupler for the Ka-band TE_{2,1} Gyro-TWT and the other is a Y-type input coupler for the K-band TE_{1,1} Gyro-TWT. For reducing the backward wave of the TE_{2,1} mode reflecting into the Y-type input coupler to influence the operating bandwidth, a Bragg reflector with a strong mode selective characteristic is inserted between these two couplers, which can make the reflection coefficient of the TE_{2,1} mode better than -1 dB and the phase matched in the whole bandwidth, and the transmission coefficient of the TE_{1,1} mode can reach better than -1 dB. Based on the simulation results, the -1 dB bandwidth of the Ka-band TE_{1,0}[□]-TE_{2,1}[○] mode input coupler reaches 3.32 GHz and the -1 dB bandwidth of K-band TE_{1,0}[□]-TE_{1,1}[○] mode input coupler reaches 3.15 GHz. The designed dual-mode input coupler has the advantages of broad bandwidth and low loss and can be well used in dual-band Gyro-TWTs.

Keywords: dual-band; Gyro-TWT; input coupler; coaxial cavity; Bragg reflector



Citation: Ma, M.; Zhao, Q.; Mo, K.; Zheng, S.; Peng, L.; Lv, Y.; Feng, J. Design of a Dual-Mode Input Structure for K/Ka-Band Gyrotron TWT. *Electronics* **2022**, *11*, 432. <https://doi.org/10.3390/electronics11030432>

Academic Editor: Gianluca Traversi

Received: 25 December 2021

Accepted: 27 January 2022

Published: 30 January 2022

Publisher's Note: MDPI stays neutral with regard to jurisdictional claims in published maps and institutional affiliations.



Copyright: © 2022 by the authors. Licensee MDPI, Basel, Switzerland. This article is an open access article distributed under the terms and conditions of the Creative Commons Attribution (CC BY) license (<https://creativecommons.org/licenses/by/4.0/>).

1. Introduction

Gyrotron traveling wave amplifiers (Gyro-TWTs) utilize the relativistic electron cyclotron maser instability to realize a high-power microwave source with high conversion efficiency [1]. Compared with solid-state devices, such as diode and semiconductor devices, which are the main microwave source in communications, low-power radar, and the field of satellite communication [2,3], Gyro-TWTs are widely used in high-power and high-resolution radar, plasma heating and electronic countermeasure [4–7]. Because of using a nonresonant fast wave structure, the Gyro-TWT features the capabilities of high-power and broad bandwidth from millimeter to submillimeter, even to terahertz band. In recent years, significant progress has been made in the development of Gyro-TWTs that are even higher power and more stable. The National Tsing Hua University reported a Ka-band TE₁₁ Gyro-TWT with off-axis electrons, which can produce 93 kW saturated peak output power at 70 dB stable gain and 26.5% efficiency with a 3 dB bandwidth of 8.6% [8]. Distributed wall losses are employed in the experiment to suppress the spurious oscillations. A Q-band TE₀₁ Gyro-TWT with an output power of 152 kW at 41 dB saturated gain was developed in the University of Electronics Science and Technology of China [9]. High harmonic large orbit Gyro-TWT amplifiers can operate at higher beam currents and have good mode selection characteristics, therefore, producing higher power [10–12]. The Institute of Applied Physics (IAP) reported a second harmonic large orbit Gyro-TWT in the Ka-band. A spiral corrugated waveguide interaction circuit was adopted to suppress mode competition. The continuous wave power can reach 7.7 kW, the 3 dB bandwidth is 2.6 GHz,

the gain is 26 dB, and the peak power reaches 180 kW [10]. Moreover, the University of Strathclyde reported a large orbit Gyro-TWT in W-band, the corresponding peak power is 3.4 kW, the gain and bandwidth are 37 dB and 5.8 GHz [12], respectively.

With the development of radar technology, advanced radar and communication systems are aiming to work in a dual-frequency band, which requires the amplifier providing the dual-band amplification to reduce in size, cost and weight in the radar transmitter system. Therefore, studying a Gyro-TWT operating at dual-band is very meaningful. As an important component of Gyro-TWTs, the input coupler that couples the EM radiation into the Gyro-TWT interaction cavity should be studied [13–19]. There are many kinds of input couplers, such as single-slit side-wall coupler, coaxial coupler, and couplers based on power splitter type. Most of the input couplers only can operate at single-mode and single frequency bands. The University of Electronic Science and Technology of China designed a Ku/Ka-band dual-frequency Gyro-TWT input coupler, but its -1 dB bandwidth is only 2 GHz [19].

In this paper, a dual-mode large bandwidth input coupler for K/Ka Gyro-TWT is theoretically designed. This structure is composed of two different types of input couplers, one is the coaxial input coupler for Ka-band $TE_{2,1}$ Gyro-TWT and the other is a Y-type input coupler for K-band $TE_{1,1}$ Gyro-TWT. For reducing the backward wave of the $TE_{2,1}$ mode reflecting into the Y-type input coupler to influence the operating bandwidth, a Bragg reflector with a strong mode selective characteristic is inserted between these two couplers. The -1 dB bandwidth of the Ka-band $TE_{1,0}^{\square}-TE_{2,1}^{\circ}$ mode input coupler is broadened to 3.32 GHz with the center operating frequency of 19 GHz and the -1 dB bandwidth of the K-band $TE_{1,0}^{\square}-TE_{1,1}^{\circ}$ mode input coupler can reach 3.15 GHz with the center operating frequency of 34 GHz. The designed input coupler could be well used in the dual-band Gyro-TWTs.

The organization of the paper is such that the single designs of coaxial and Y-type input couplers are discussed in Section 2. The Bragg reflector is also described in detail. The design of a dual-band input coupler is presented in Section 3, including the isolation between these two couplers. The summary is given in Section 4.

2. Design of Input Coupler

Two types of input couplers are discussed in this section, one is based on coaxial coupling [20], which converts the $TE_{1,0}^{\square}$ mode of the rectangular waveguide to the $TE_{2,1}^{\circ}$ mode of circular waveguide in the Ka-band and the other is based on Y-shape input couplers [21], which can transform the $TE_{1,0}^{\square}$ to $TE_{1,1}^{\circ}$ in the K-band.

2.1. Input Coupler Based on Coaxial Coupling Cavity

Figure 1 shows the schematic diagram of the coaxial input couple, where r_a is the inner radius of the coaxial resonator, r_b is the outer radius of the coaxial resonator, r_c is the radius of the cut-off waveguide. Generally, r_c is about 0.7–0.8 times the size of r , which is the output waveguide radius. Port 1 is the standard rectangular waveguide port where $TE_{1,0}^{\square}$ is feed into, port 4 is the output port where $TE_{2,1}^{\circ}$ is transmitted to the interaction cavity, port 3 is the cut-off port to prevent the EM radiation into the gun section. When $TE_{1,0}^{\square}$ is coupled to the coaxial resonator cavity, the $TE_{4,1,1}$ mode is excited in the coupled cavity [22]. There are four coupling rectangular slits between the coaxial resonator and the cylindrical cavity. Therefore, the $TE_{4,1,1}$ mode can be coupled to $TE_{2,1}^{\circ}$.

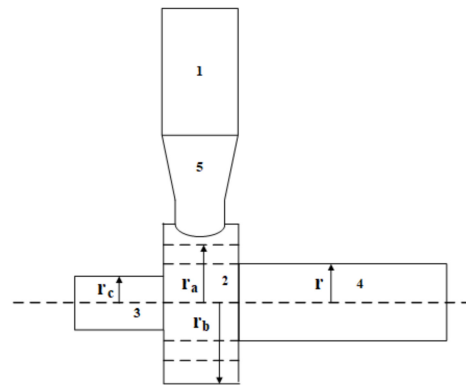


Figure 1. Schematic diagram of the coaxial input coupler.

It is necessary to study the Eigenvalue equation and propagation characteristics of the TE mode before designing the coupler, where the TE mode is only considered in the coaxial resonator. The longitudinal field component of the TE mode propagating in the axial waveguide is [13]:

$$H_z = K_c^2 [C_m J_m(K_c r) + D_m Y_m(K_c r)] \sin m\varphi e^{-j\beta z} \tag{1}$$

where K_c is the cut-off wave number, m is the angular index of $TE_{m,n}$, $J_m(x)$ and $Y_m(x)$ are the m^{th} order Bessel function and Neumann function, C_m and D_m are the mode amplitude.

From the boundary condition $\frac{\partial H_z}{\partial r} |_{r=a,b} = 0$, a homogeneous linear system of equations about C_m and D_m is obtained as:

$$\begin{cases} C_1 J'_m(K_c r_a) + D_1 Y'_m(K_c r_a) = 0 \\ C_2 J'_m(K_c r_b) + D_2 Y'_m(K_c r_b) = 0 \end{cases} \tag{2}$$

If there exists a non-zero solution of (2), the determinant is equal to zero, so the Eigenvalue equation of the $TE_{m,n}$ mode can be obtained as below

$$J'_m(\chi_{m,n}) Y'_m(\alpha \chi_{m,n}) - J'_m(\alpha \chi_{m,n}) Y'_m(\chi_{m,n}) = 0 \tag{3}$$

where $\chi_{m,n} = K_c r_a$ is the root of the Eigenvalue equation, $\alpha = r_b/r_a$ is the ratio of the inner and outer radius of the coaxial cavity. The propagation constant β_{mn} and resonance conditions of the TE_{mn} modes in coaxial waveguides are obtained as shown in (4) and (5):

$$\beta_{mn} = \sqrt{K^2 - K_c^2} = \sqrt{\omega^2 \epsilon \mu - (\chi_{mn}/r_a)^2} \tag{4}$$

$$\beta_{mn} L = p\pi (p = 1, 2, 3 \dots) \tag{5}$$

where L is the length of the coaxial resonator. By solving the Eigenvalue Equation (3) numerically, the relationship between the eigenvalue and the ratio of the inner and outer radius of the coaxial waveguide is obtained.

As shown in Figure 2, the Eigenvalue reduces with the rise of the ratio. To increase the coupling between the inner and outer cavity and reduce the size of the coupler, the thickness of the coupling silt is always 0.3~0.5 mm. Based on the results from a beam-wave interaction and the results in Figure 2, the geometric configuration of the input coupler is preliminary determined. Then, with the help of CST (in the simulation, the resolution is set as -40 dB), the structure of the input coupler is optimized and the field distribution at the frequency of 34 GHz is plotted in Figure 3. It is obvious that $TE_{2,1}^O$ is excited at the circular cavity.

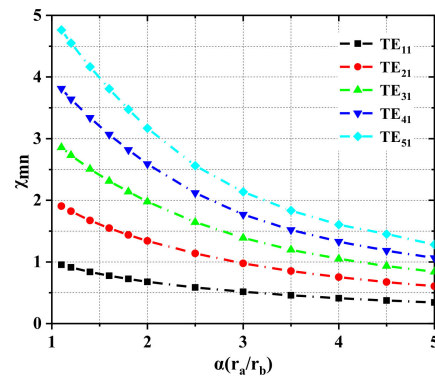


Figure 2. The relationship between the Eigenvalue root $\chi_{m,n}$ and the inner coaxial cavity and outer coaxial cavity radii ratio a .

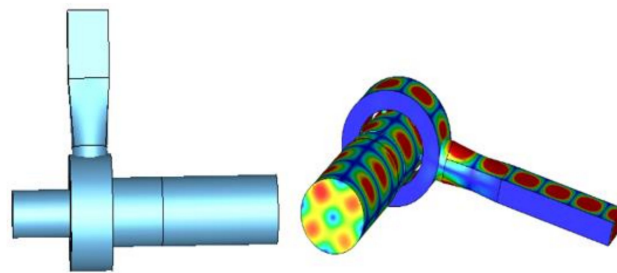


Figure 3. Coupler structure and field distribution diagram.

The influence of the width of the coupling rectangular gap on the transmission and reflection of the input coupler is plotted in Figure 4. It is found that the reflection coefficient increases slightly with the rise of the coupling gap width. Whereas the transmission is almost unchanged in the frequency range of 33–38 GHz. Figure 5 shows the influence of the coupling rectangular gap length on the performance of the input coupler. It can be seen that the transmission remains unchanged in the frequency range of 33–38 GHz when the gap length is increased. From the above analysis, the -1 dB bandwidth of the transmission can reach 4.30 GHz, and the reflection in the bandwidth are all below -15 dB. For reducing the reflection between the input rectangular and the coaxial cavity, a smooth variation section with a length of 10 mm is designed.

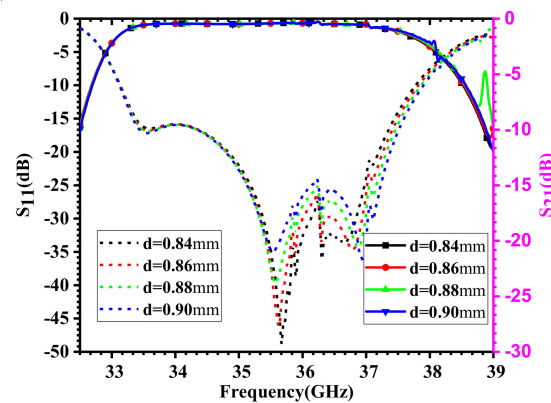


Figure 4. The influence of the coupling rectangle gap width on transmission and reflection of the input coupler.

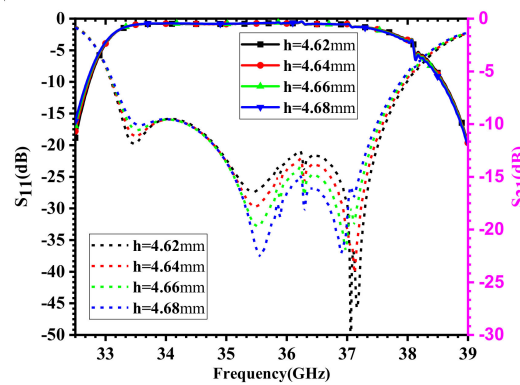


Figure 5. The influence of the coupling rectangle gap length on transmission and reflection of the input coupler.

2.2. Input Coupler Based on Side Wall COUPLING Mode

Mode $TE_{1,1}^{\circ}$ is selected as the operating mode for Gyro-TWT in the K-band. We adopt the input coupler based on sidewall coupling, as shown in Figure 6. As we know, the circularly polarized TE_{11} mode can be synthesized from two same amplitude linearly polarized TE_{11} modes with a 90-degree phase difference [21]. Therefore, the coupler has two rectangular branches to generate two linearly polarized TE_{11} modes. The simulated electric field is shown in Figure 6. It is shown that $TE_{1,1}^{\circ}$ can be excited in the circular cavity. The input rectangular waveguide is the waveguide standard BJ180. The circular waveguide is 5.1 mm, which is the same as the radius of the output cavity of the coaxial coupler. In addition, a tapered geometry with a length of 4 mm is used between the output rectangular waveguide and the circular waveguide to effectively reduce the reflection. The transmission and reflection are plotted in Figure 7. The frequency range of -1 dB bandwidth can reach 17.5~21.4 GHz, the bandwidth is 3.9 GHz.

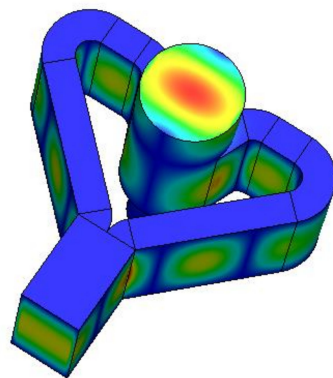


Figure 6. Geometric structure of the Y-type input coupler.

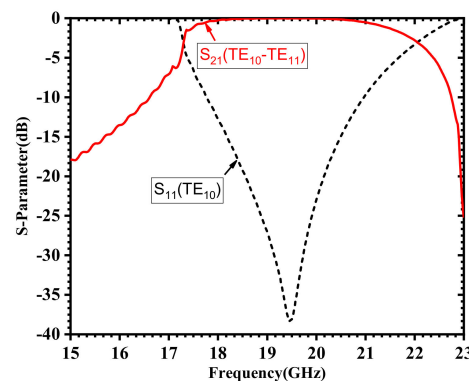


Figure 7. Simulation results of the Y-type input coupler.

2.3. Bragg Reflector

The cut-off waveguide is a general solution to improve the transmission coefficient for the input coupler. The only requirement is the radius of the cut-off waveguide needs to be sufficiently small. Thus, the radius of the cut-off waveguide in the coaxial cavity is 3.50 mm, which is smaller than the radius of the output cavity. To solve this problem, a Bragg reflector with a strong mode selection feature is adopted to connect the output end of the Y-type input coupler and the cut-off port of the coaxial input coupler [23–26]. The function of the Bragg reflector is to allow the $TE_{1,1}^{\circ}$ mode transmission with no reflection and prevent the $TE_{2,1}^{\circ}$ mode transmitting into the Y-type coupler. The Bragg reflectors can be constructed in a variety of ways, among the various axial periodic structures, the simplest structure is the periodic rectangular-corrugation waveguide, which includes two circular waveguide sections with different radii in one period. According to the Bragg resonance conditions given in [23] ($2k = k_b$, where k is the axial propagation constant of the wave, $k_b = 2\pi/l$, l is the corrugation period), the geometric structure of the Bragg reflector is determined and a strong mode-selective reflection that scatters the incident wave coherently into a backward wave can be achieved. It was shown that the bandwidth of the Bragg reflector can be improved by varying the corrugation profile. As shown in Figure 8, a seven-section reflector was designed to operate in the frequency range of 33~38 GHz and 17.5~21.4 GHz. The minimum radius of the reflector R_{in} is the same as the radius of the interaction zone. Based on the joint simulation of CST and MATLAB, the length of each section is shown in Table 1. The outer radius R_{out} is 11.63 mm. Figure 9 shows the reflection coefficient and phase of the $TE_{2,1}^{\circ}$ mode. The results show that the reflector achieves total reflection in the frequency range of 33~38 GHz, the phase spread can be even smaller, and the transmission S_{21} in the frequency range of 17.5~21.4 GHz is close to 0 dB and the corresponding reflection S_{11} is below -10 dB. The designed reflector satisfies the dual-band input coupler.

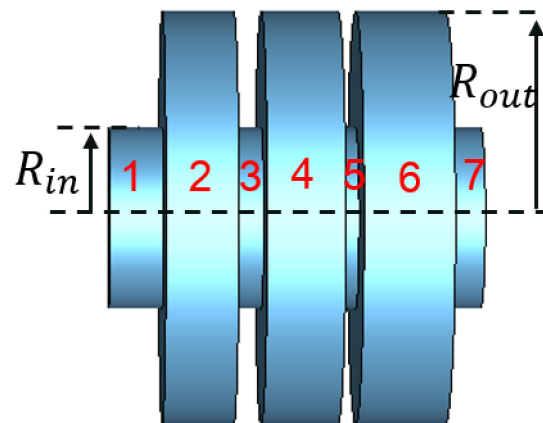


Figure 8. Structure diagram of the Bragg reflector.

Table 1. Dimensions of the Bragg reflector.

Section Number	Length (mm)
1	3
2	4
3	1.6
4	4.3
5	1.5
6	4.3
7	2

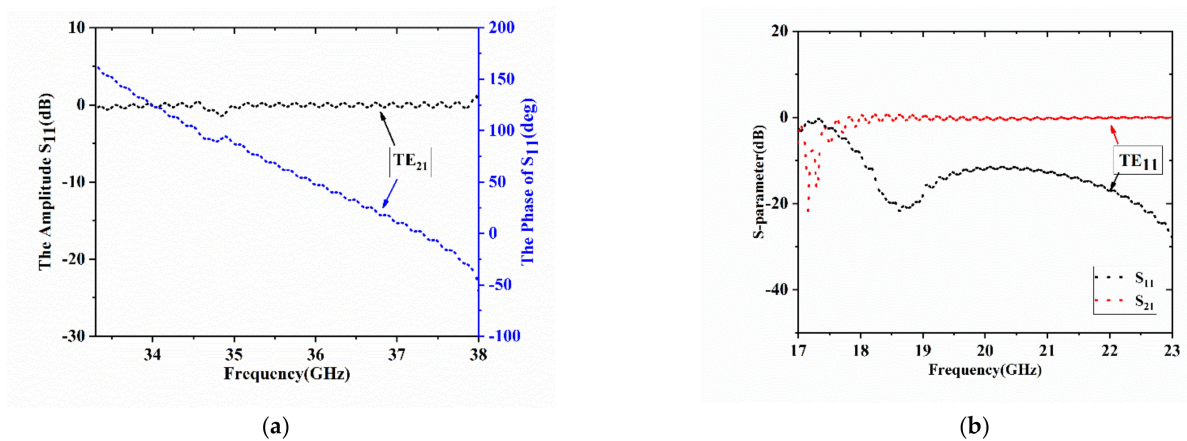


Figure 9. (a) Reflection amplitude (the black-dot curve) and phase (the blue-dot curve) of S_{11} of $TE_{1,1}^{\square}$ mode, (b) the reflection and transmission of $TE_{1,1}^{\square}$ mode.

3. Simulation of Dual-Mode Input Couplers

Based on the front studies, a dual-input coupler for K/Ka dual-band Gyro-TWT is designed, as shown in Figure 10. Port 1 is the input port for $TE_{1,0}^{\square}$ in the K-band, port 2 is the input port for $TE_{1,0}^{\square}$ in the Ka-band, port 3 is the output port with a radius of 5.1 mm, Section 4 is the Bragg reflector, and port 5 is the cut-off port. Figure 11 shows the electric field distribution of the input coupler when the operating mode is $TE_{1,1}^{\square}$ at a frequency of 18 GHz and the $TE_{2,1}^{\square}$ at a frequency of 34 GHz. It can be seen that the electric field is blocked in the Bragg reflector and no field is transmitting into the Y-type input coupler when the dual-mode input coupler is operating at $TE_{2,1}^{\square}$, and the Bragg reflector has no influence on the transmission of $TE_{1,1}^{\square}$. Figures 12 and 13 plot the S-parameter and phase of the designed dual-mode input coupler in the K/Ka-band. It is shown that the reflection coefficient in the frequency range of 18.3~21 GHz is below -10 dB when the output mode is $TE_{1,1}^{\square}$, the -1 dB bandwidth of transmission can reach 3.15 GHz. Meanwhile, the reflection coefficient in the frequency range of 33.7~37.2GHz is below -10 dB when the output mode is $TE_{2,1}^{\square}$, and the -1 dB bandwidth is 3.32 GHz. The comparison between the presented input coupler and that in [19] is shown in Table 2. It can be seen that the input coupler bandwidth is relatively broadened to wide. The designed input coupler can be used as a dual-band large bandwidth Gyro-TWT.

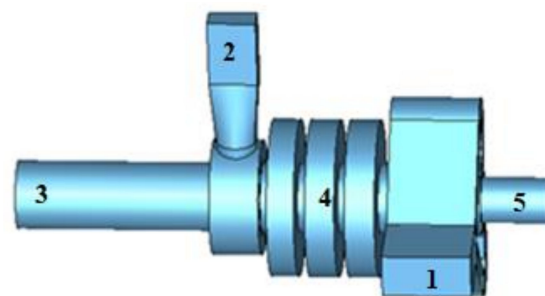


Figure 10. Structure diagram of dual-frequency input coupler (1 is the input port for $TE_{1,1}^{\square}$ in K-band, 2 is the input port for $TE_{1,1}^{\square}$ in Ka-band, 3 is the output port, 4 is the Bragg reflector, 5 is the cut-off port).

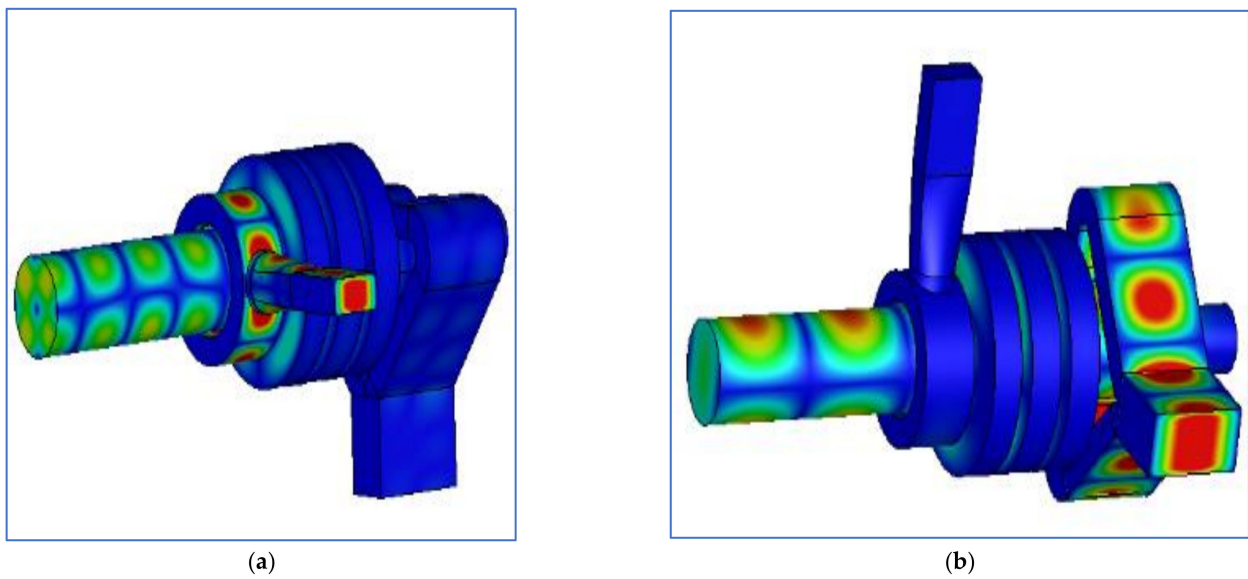


Figure 11. The electric field diagram of input coupler, (a) the output mode is $TE_{1,1}^{\circ}$, (b) the output mode is $TE_{1,1}^{\circ}$.

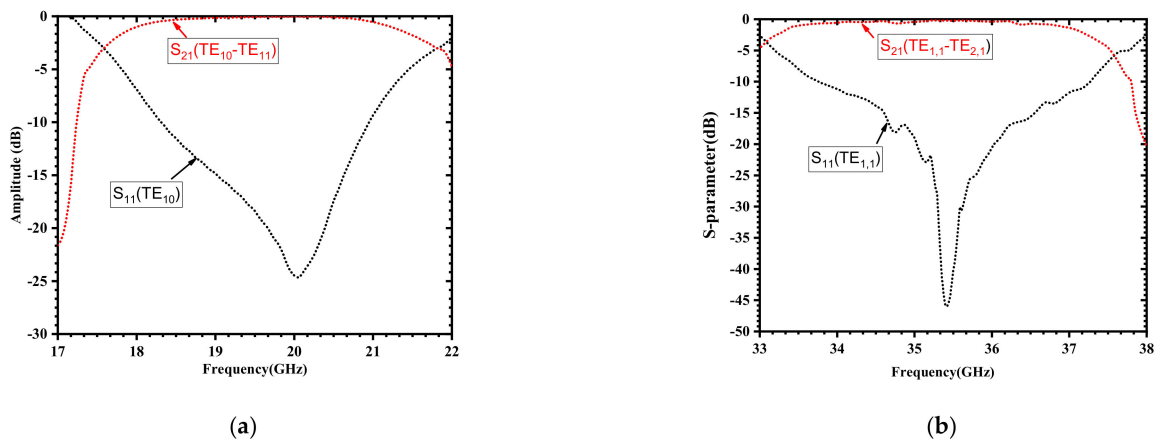


Figure 12. The S-parameter for the designed dual-mode input coupler, (a) the S-parameter when the output mode is $TE_{1,1}^{\circ}$, (b) the S-parameter when the output mode is $TE_{2,1}^{\circ}$.

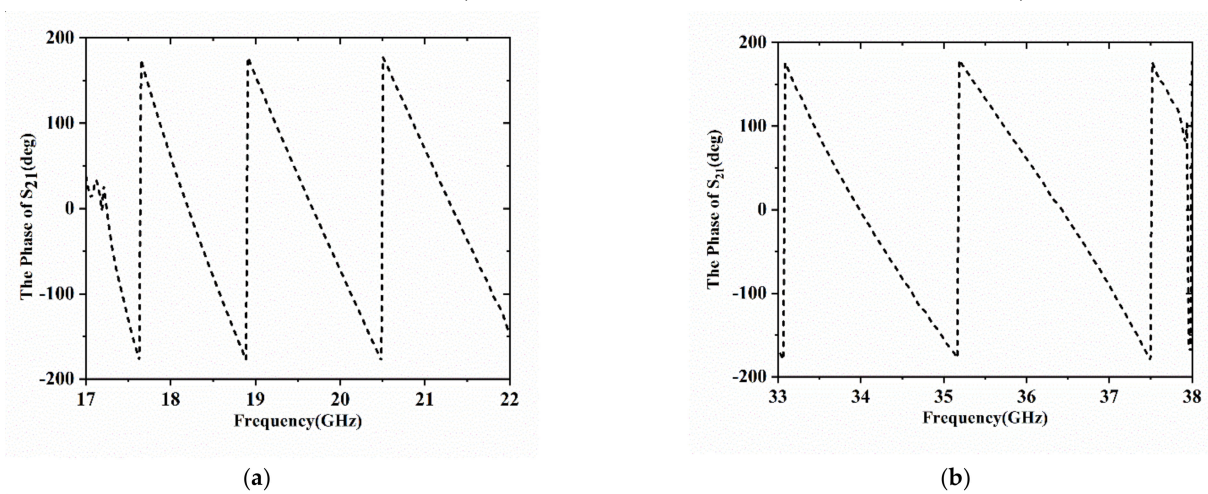


Figure 13. The phase of S_{21} for the designed dual-mode input coupler, (a) the phase of S_{21} when the output mode is $TE_{1,1}^{\circ}$, (b) the phase of S_{21} when the output mode is $TE_{2,1}^{\circ}$.

Table 2. The dual-band input coupler parameters.

Parameters	This Article	Reference [19]
Operating Frequency	19/34GHz	17/33GHz
Operating Mode	$TE_{1,0}^{\square}-TE_{2,1}^{\circ}$ @ Ka-band and $TE_{1,0}^{\square}-TE_{1,1}^{\circ}$ @ K-band	$TE_{1,0}^{\square}-TE_{0,1}^{\circ}$ @ Ka-band and $TE_{1,0}^{\square}-TE_{1,1}^{\circ}$ @ K-band
−1 dB Bandwidth	3.15 GHz @ K-band, 3.32 GHz @ Ka-band	1.9 GHz @ K-band, 2 GHz @ Ka-band

Figure 14 plots the isolation between the two input rectangular waveguides when the designed dual-mode input coupler is operating at K-band and Ka-band, respectively. When the coupler is operating in the K-band, the isolation of the $TE_{1,1}^{\circ}$ mode is below -40 dB in the 17~22GHz frequency range. When operating in the Ka-band, the isolation of the $TE_{2,1}^{\circ}$ mode is below -20 dB in the frequency range of 33~38 GHz. Through these analyses, it is proved that the designed input coupler has good properties for single-mode operating.

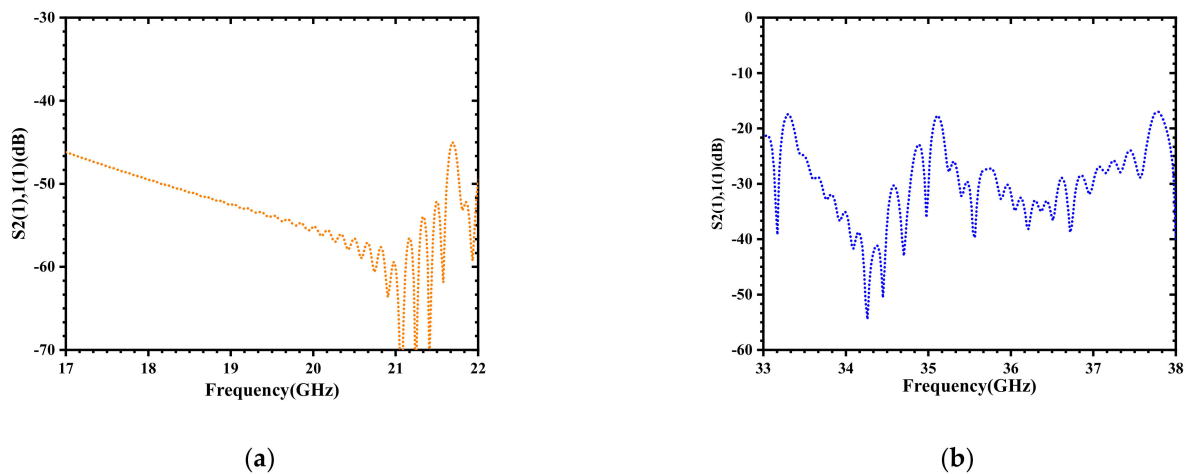


Figure 14. The isolation between the input rectangular (a) port 1 and (b) port 2 (ports 1 and 2 are labeled in Figure 10).

4. Conclusions

Dual-band Gyro-TWTs can be used in new radars, communication systems and other fields to achieve cross-band operation requirements. In this paper, a Gyro-TWT input coupler for dual-band operation is presented. The coupler realizes the transition from the rectangular waveguide mode to the circular waveguide mode in different wavebands. The designed structure is composed of two different types of input couplers, one is the coaxial input coupler for the Ka-band $TE_{2,1}^{\circ}$ Gyro-TWT and the other is a Y-type input coupler for the K-band $TE_{1,1}^{\circ}$ Gyro-TWT. For reducing the reflection wave from $TE_{2,1}^{\circ}$ reflecting into the Y-type input coupler to influence the operating bandwidth, a Bragg reflector is inserted to connect these two couplers. Through optimization, the -1 dB bandwidth of the dual-band input coupler can achieve 3.15 GHz in the K-band with the output mode of $TE_{1,1}^{\circ}$ and 3.32 GHz in the Ka-band with the output mode of $TE_{2,1}^{\circ}$. Meanwhile, the isolation degree of the two input rectangular ports is below -20 dB. The designed dual-mode input coupler can be well used for dual-band Gyro-TWTs.

Author Contributions: Conceptualization, M.M. and Q.Z.; methodology, M.M., L.P.; resources, S.Z., K.M., Y.L. and J.F.; data curation, Q.Z.; formal analysis, Q.Z., J.F.; writing—original draft preparation, M.M. and Q.Z.; writing—review and editing, Q.Z., J.F.; funding acquisition, Q.Z., J.F. All authors have read and agreed to the published version of the manuscript.

Funding: This research was funded by the National Natural Science Foundation of China: 62001131, the Dean Project of Guangxi Key Laboratory of Wireless Broadband Communication and Signal Processing Grant Nos: GXKL06190102, the Guangxi Natural Science Foundation Project: 2019GXNSFBA245066, and the Guangxi Science and Technology Base and Talent Special Project: AD19245042.

Conflicts of Interest: The authors declare no conflict of interest.

References

1. Chu, K.R.; Lin, A.T. Gain and bandwidth of the Gyro-TWT and CARM amplifiers. *IEEE Trans. Plasma Sci.* **1988**, *16*, 90–104. [[CrossRef](#)]
2. Li, H.H.; Wang, K.S.; Zhao, J.X.; Xiao-xin, L.I.A.N.G.; Yue-peng, Y.A.N. A design of Ka-band power amplifier based on 0.15 μm GaAs pHEMT process. *Microelectron. Comput.* **2021**, *38*, 17–21.
3. Hosseinzadeh, N.; Medi, A. Wideband 5 W Ka-Band GaAs Power Amplifier. *IEEE Microw. Wirel. Compon. Lett.* **2016**, *26*, 1–3. [[CrossRef](#)]
4. Chu, K.R. Overview of Research on the gyrotron traveling-wave amplifier. *IEEE Trans Plasma Sci.* **2002**, *30*, 903–908.
5. Baik, C.-W.; Jeon, S.-G.; Kim, D.-H.; Sato, N.; Yokoo, K.; Park, G.-S. Third-harmonic frequency multiplication of a two-stage tapered gyrotron TWT amplifier. *IEEE Trans. Electron Devices* **2005**, *52*, 829–838. [[CrossRef](#)]
6. Linde, G.J.; Ngo, M.T.; Danly, B.G.; Cheung, W.J.; Gregers-Hansen, V. WARLOC: A high-power coherent 94 GHz radar. *IEEE Trans. Aerosp. Electron. Syst.* **2008**, *44*, 1102–1117. [[CrossRef](#)]
7. Paoloni, C.; Gamzina, D.; Letizia, R.; Zheng, Y.; Luhmann, N.C., Jr. Millimeter wave traveling wave tubes for the 21st Century. *J. Electromagn. Waves Appl.* **2021**, *35*, 567–603. [[CrossRef](#)]
8. Chu, K.R.; Chen, H.Y.; Hung, C.L.; Chang, T.-H.; Barnett, L.; Chen, S.-H.; Yang, T.-T.; Dialetis, D.J. Theory and experiment of ultrahigh-gain gyrotron traveling wave amplifier. *IEEE Trans. Plasma Sci.* **1999**, *27*, 391–404.
9. Yan, R.; Luo, Y.; Liu, G.; Pu, Y. Design and experiment of a Q-band gyro-TWT loaded with lossy dielectric. *IEEE Trans. Electron. Devices* **2012**, *59*, 3612–3617. [[CrossRef](#)]
10. Samsonov, S.V.; Gachev, I.G.; Denisov, G.G.; Bogdashov, A.; Mishakin, S.V.; Fiks, A.S.; Soluyanov, E.A.; Tai, E.M.; Dominyuk, Y.V.; Levitan, B.A.; et al. Ka-Band gyrotron traveling-wave tubes with the highest continuous-wave and average power. *IEEE Trans. Electron. Devices* **2014**, *61*, 4264–4267. [[CrossRef](#)]
11. Harriet, S.B.; McDermott, D.B.; Gallagher, D.A.; Luhmann, N. Cusp Gun TE₂₁ Second-Harmonic Ka-Band Gyro-TWT Amplifier. *IEEE Trans. Plasma Sci.* **2002**, *30*, 909–914. [[CrossRef](#)]
12. He, W.; Donaldson, C.R.; Zhang, L.; Ronald, K.; Phelps, A.D.R.; Cross, A.W. Broadband amplification of low terahertz signals using axis-encircling electrons in a helically corrugated interaction region. *Phys. Rev. Letts.* **2017**, *119*, 184801. [[CrossRef](#)] [[PubMed](#)]
13. Xu, Y.; Xiong, C.D.; Yong, L.; Jianxun, W.; Ran, Y.; Youlei, P.; Wang, H.; Li, H. Design of broad-band input coupler of Ka-band TE₀₁ mode gyro-TWT. *Chin. J. Vac. Sci. Technol.* **2012**, *32*, 208–213.
14. Xiong, W.J.; Wang, L.; Luo, Y.; Guo, L. Improved design of input and output structures of W band gyro-TWT. *High Power Laser Part. Beams* **2013**, *25*, 693–698. [[CrossRef](#)]
15. Wang, Q.S.; Huey, H.E.; McDermott, D.B.; Hirata, Y.; Luhmann, N. Design of a W-band Second-harmonic TE₀₂ gyro-TWT amplifier. *IEEE Trans. Plasma Sci.* **2000**, *28*, 2232–2238. [[CrossRef](#)]
16. McDermott, D.B.; Song, H.H.; Hirata, Y.; Lin, A.T.; Barnett, L.R.; Chang, T.H.; Hsu, H.-L.; Marandos, P.S.; Lee, J.; Chu, K.R.; et al. Design of a W-band TE₀₁ mode gyrotron traveling-wave amplifier with high power and broad-band capabilities. *IEEE Trans. Plasma Sci.* **2003**, *30*, 894–902. [[CrossRef](#)]
17. Liu, G. Input coupler design for Ka band gyrotron TWT. In Proceedings of the 2016 IEEE International Vacuum Electronics Conference (IVEC), Monterey, CA, USA, 19–21 April 2016; pp. 1–2.
18. Zhang, L.; He, W.; Donaldson, C.; Garner, J.R.; McElhinney, P.; Cross, A.W. Design and Measurement of a Broadband Sidewall Coupler for a W-Band Gyro-TWA. *IEEE Trans. Microw. Theory Tech.* **2015**, *63*, 3183–3190. [[CrossRef](#)]
19. Sun, M. *Research on the Transmission Link of Gyro-TWT Input and Output System [D]*; University of Electronic Science and Technology of China: Chengdu, China, 2019; pp. 34–65.
20. Xu, Y.; Li, Y.; Wang, J.X.; Jiang, W.; Liu, G.; Luo, Y.; Li, H. Design and experiment of a high power and broadband Ku-Band TE₁₁ mode Gyro-TWT. *IEEE Trans. Electron. Devices* **2018**, *66*, 1559–1566. [[CrossRef](#)]
21. Yu, C.F.; Chang, T.H. High-performance circular TE₀₁-mode converter. *IEEE Trans. Microw. Theory Tech.* **2005**, *53*, 3794–3798.
22. Collin, R.E. *Field Theory of Guided Waves*; Wiley Interscience: New York, NY, USA, 1990; pp. 415–420.
23. Chong, C.K.; McDermott, D.B.; Razeghi, M.M.; Luhmann, N.C.; Pretterebner, J.; Wagner, D.; Thumm, M.; Caplan, M.; Kulke, B. Bragg reflectors. *IEEE Trans. Plasma Sci.* **1992**, *20*, 393–402. [[CrossRef](#)]

24. Peskov, N.Y.; Ginzburg, N.S.; Kaminskii, A.A.; Kaminskii, A.K.; Sedykh, S.N.; Sergeev, A.P.; Sergeev, A.S. High-efficiency narrow-band free-electron maser using a Bragg cavity with a phase discontinuity in the ripples. *Tech. Phys. Lett.* **1999**, *25*, 429–432. [[CrossRef](#)]
25. Emile, D.R. Innovative corrugated transmission line for Terahertz wave-guiding. In Proceedings of the 2011 International Conference on Infrared, Millimeter, and Terahertz Waves, Houston, TX, USA, 2–7 October 2011; pp. 1–2.
26. Wenzel, H.; Guther, R.; Shams-Zadeh-Amiri, A.M.; Bienstman, P. A comparative study of higher order Bragg gratings: Coupled-mode theory versus mode expansion modeling. *IEEE J. Quantum Electron.* **2006**, *42*, 64–70. [[CrossRef](#)]